Self-consistent pseudopotential calculations for Ge and diamond (111) surfaces*

J. Ihm, Steven G. Louie,[†] and Marvin L. Cohen

*Department of Physics and Materials and Molecular Research Division,
Lawrence Berkeley Laboratory, Berkeley, California 94720*

(Received 16 August 1977)

The self-consistent pseudopotential method with a slab geometry is applied to electronic structure calculations of the Ge and diamond (111) surfaces. A nonlocal pseudopotential is derived and found to produce an energy band structure of bulk diamond in good agreement with other calculations and experiments. This potential is then used for the diamond surface calculations. The calculations are restricted to unrelaxed, unreconstructed surfaces. Various surface states are identified and discussed.

I. INTRODUCTION

In this paper we present the results of calculations of the electronic structure of the Ge and diamond (111) surfaces using a self-consistent pseudopotential method.[1] Only clean, unrelaxed, and unreconstructed surfaces are examined. Although this assumption may be unrealistic compared with various experiments[2-6] which more or less support an inward relaxation of surface atoms and a 2×1 or a 2×8 reconstruction for Ge depending on experimental circumstances, the results for this ideal case reveal many of the physically interesting phenomena occurring on the surface. Furthermore, these results can be used for comparison with calculations involving more complicated geometries and also with interface problems.

Details of the present method are discussed extensively elsewhere,[1] hence, only brief outlines of the calculational procedure are given below. The one-electron Schrödinger equation is solved with a pseudopotential Hamiltonian

$$H = p^2/2m + V_{ps} + V_H + V_x . \tag{1}$$

V_{ps} is a total pseudopotential taken to be a superposition of ionic pseudopotentials V_{ion} representing Ge^{4+} or C^{4+} core,

$$V_{ps}(\vec{r}) = \sum_{\vec{R}n,\vec{\tau}i} V_{ion} (\vec{r} - \vec{R}_n - \vec{\tau}_i) \tag{2}$$

where the $\vec{R}_n$'s and $\vec{\tau}_i$'s are the lattice vectors and the basis vectors in the primitive cell, respectively. The ionic pseudopotential is screened by adding a Hartree potential V_H and a local exchange potential V_x obtained from the charge density ρ by

$$\nabla^2 V_H (\vec{r}) = -4\pi e^2 \rho(\vec{r}) \tag{3}$$

and

$$V_x(\vec{r}) = -3e^2(3/8\pi)^{1/3} \alpha \rho(\vec{r})^{1/3} . \tag{4}$$

In the present work, the value of the exchange

parameter α is chosen to be 0.794 to make possible a direct comparison with similar work for the Si (111) surface and the Ge (111) relaxed surface[9] using the same α.

The self-consistent iteration procedure is initiated by approximating the $(V_{ps} + V_H + V_x)$ term in the Hamiltonian by an empirical pseudopotential constructed from a superposition of atomic pseudopotentials. With this Hamiltonian, the valence charge distribution is calculated and from it the screening potentials V_H and V_x are obtained. V_H and V_x are then put back into the Hamiltonian (1). The procedure is repeated until self-consistency is reached, i.e., until the input and the output screening potentials $(V_H + V_x)$ agree with each other. The wave functions are expanded solely in terms of plane waves. This basis set of plane waves was shown to successfully represent charge distributions of covalent bonding materials with a relatively small number of waves.[7]

In Sec. II, the Ge (111) surface results are reported. In Sec. III, a nonlocal pseudopotential for carbon is obtained and tested for the bulk band structure of diamond. The electronic structure of the diamond (111) surface is presented and discussed in Sec. IV, and some summarizing remarks and conclusions are given.

II. Ge (111) SURFACE

In this work the (local) ionic pseudopotential of Appelbaum and Hamann [8](AH) is employed to facilitate comparison of our results with calculations for the relaxed surface done by Chelikowsky[9] using the same potential,

$$V_{ion} (\vec{q}) = \frac{e^2}{\Omega_{atom}} \left[-\frac{4\pi z}{q^2} + \left(\frac{\pi}{\alpha}\right)^{3/2} \nu_1 \right.$$
$$\left. + \left(\frac{\pi}{\alpha}\right)^{3/2} \left(\frac{3}{2\alpha} - \frac{q^2}{4\alpha^2}\right)\nu_2 \right] \exp\left(-\frac{q^2}{4\alpha}\right), \tag{5}$$

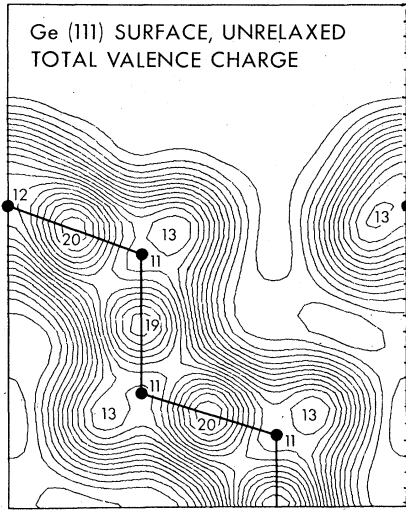where Ω_{atom} is the cell volume per atom, $z = 4$,

FIG. 1. Total valence charge distribution for an un-relaxed Ge (111) surface. The charge density is plotted as contour in a $(1\bar{1}0)$ plane intersecting the (111) surface at right angles. The plotting area starts in the vacuum and extends $4\frac{1}{2}$ atomic layers into the crystal. The nor-malization is in terms of the number of electrons per bulk unit cell volume $\Omega_c = \frac{1}{4}a_c^3$.

$\alpha = 0.61$, $\nu_1 = 2.64$, and $\nu_2 = -1.237$, respectively. This potential gives energy levels of the Ge atom in agreement (up to a few tenths of an eV) with Herman and Skillman.[16]

As in the Si (111) surface calculation of Ref. 1, we retain the periodicity of the system along the direction perpendicular to the surface using "supercells" of repeated slabs. The "supercell" consists of 12 Ge layers and a vacuum region equivalent to 5 layers in thickness. The slab thickness and the separation between slabs are large enough to prevent any significant interactions be-tween neighboring surfaces. Ω_{atom} is $216.45a_{\text{Bohr}}^3$ for the present geometry. Nearly 200 plane waves are used for the expansion of the wave functions and another ~250 plane waves are included through Löwdin's perturbation scheme.[10] These values correspond to cutoff energies of 2.6 and 5.0 Ry, respectively. Most of our results are given using the figures described below.

Figure 1 shows the total (valence) charge density in a $(1\bar{1}0)$ plane cutting the (111) surface at right angles. We calculate wave functions at 28 points in the irreducible Brillouin zone (BZ) ($\frac{1}{12}$ of the first BZ in the present geometry) and add all charge density contributions from each band up to the Fermi energy E_F. The atomic positions are indicated by dots. Moving into the crystal, the charge distribution closely resembles the Ge bulk charge density, whereas it decays rapidly
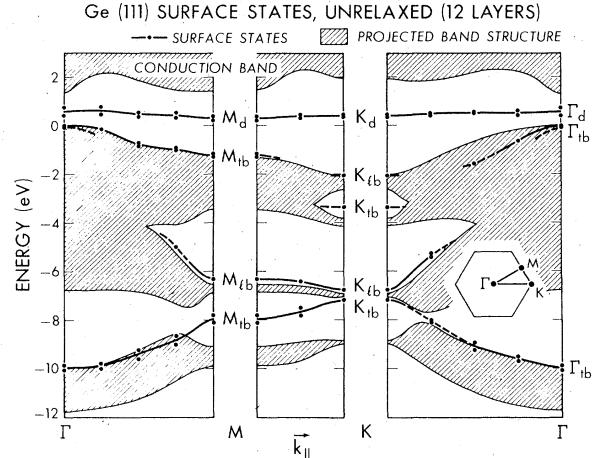

FIG. 2. Two-dimensional band structure of a 12-layer Ge (111) slab along symmetry lines. Various surface states or surface resonances are indicated by heavy lines and are labeled. Dashed lines mean "weak" sur-face states or resonances which have a long decay length into the bulk. Subscripts represent a "dangling bond (d)," a "transverse back bond (tb)," or a "longitudinal back bond (1b)," respectively. Heavy dots refer to the calculated energy eigenvalues of surface states. As a slab has two surfaces, the surface states come in pairs. Some of them are not completely degenerate due to the finite thickness. The projected band structure is also plotted. A picture of the BZ is inserted.
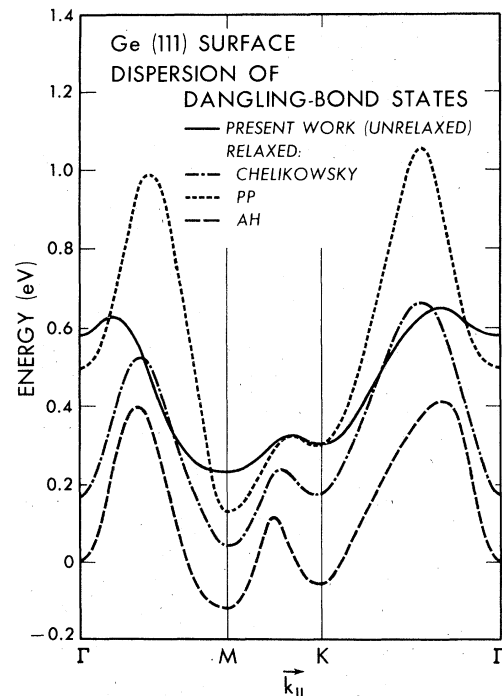

FIG. 3. Energy dispersion curves of the dangling-bond surface states in the gap. Also displayed are the results of Refs. 8, 9, and 14 for the relaxed surface.
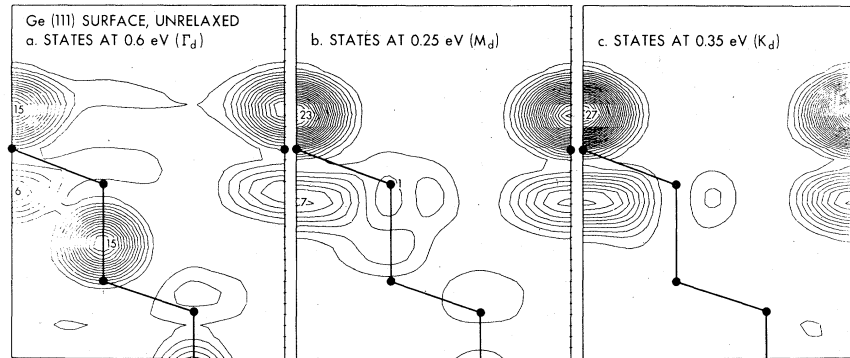
FIG. 4. Charge-density contour plots for dangling-bond states at Γ, M, and K. Indicated values are normalized to the number of electrons per unit "supercell" volume.

into the vacuum near the surface region. We can calculate the work function from the relation

$$W = V_{\text{vacuum}} - E_F,\qquad (6)$$

where V_{vacuum} refers to the total potential in the region far from the surface so that the potential is actually a constant. The value we obtained is 4.5 eV, which is in good agreement with the experimental values ranging from 4.6 to 4.9 eV.[11,12]

In Fig. 2, the two-dimensional band structure is shown along the symmetry lines in the BZ. Various surface states are labeled. The projected band structure[13] of Ge bulk in the (111) direction calculated using the same potential is also plotted as a background. The details of the dispersion curve of the dangling-bond states in the gap are given in Fig. 3, together with those obtained by other authors[8,9,14] for the relaxed surface. The overall comparison is good although our result is

for the unrelaxed surface. Chelikowsky's result for the relaxed surface[9] using the same potential and the same method as ours indicates that the bandwidth increases slightly (~0.2 eV) and the valley at Γ gets deeper by 0.3 eV when the surface is relaxed.

Contour plots of charge density of surface states are given in Figs. 4–6. We see a close resemblance between these results for Ge and the similar calculations for Si.[1] Transverse back-bond states in the upper valence band exist almost everywhere in the BZ. The energy level Γ_{tb} lies within 0.1 eV of E_v. This is in contrast to Si[1] where it is found nearly 1 eV below E_v.[1] Plots for the back-bond surface states in the lower valence band are omitted. They are localized near the bonding sites and decay rather slowly into the bulk region. The transverse back-bond surface states (tb) in the lower valence band (at −10 eV ~ −7 eV) are found and indicated in Fig. 2. These states are, however, not observable either in
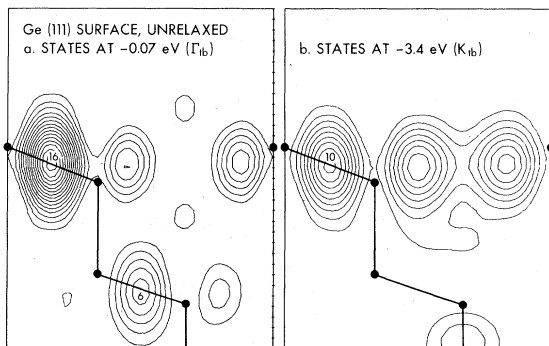

FIG. 5. Charge-density contour plots for back-bond states in the upper valence band at Γ and K. Only one of the doubly degenerate surface states at Γ is shown. The states at M are the same as at Γ, so the corresponding plot is omitted. Note that Γ_{tb} is within 0.1 eV of E_v.
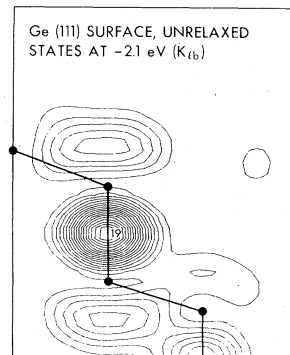

FIG. 6. Charge-density contour plot for the longitudinal back-bond states at K. These longitudinal back-bond states are found at K only.
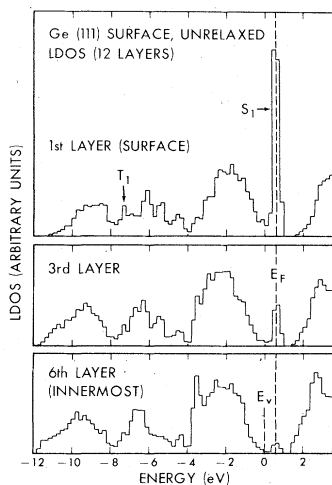
FIG. 7. Local density of states (LDOS) curves for Ge (111) slab. The surface states T_1 and S_1 are described in the text. E_v denotes the top of the bulk valence band and the Fermi energy E_F falls in a region of large density of surface states.

Si[1], or diamond (Sec. IV of the present paper), due to the fact that the potentials are stronger in those materials than in the Ge case.

Finally, the local density of states (LDOS) of each region of the slab is shown in Fig. 7. The peak at the gap denoted by S_1 is observed in the energy-loss spectroscopy.[6] This peak mainly consists of dangling-bond surface states existing throughout the Brillouin zone. Some contributions come from the transverse back-bond states localized just below the surface. E_F falls in this peak so that the ideal surface would be metallic. This figure can be compared with Figs. 2–4 in Ref. 15 where the tight-bonding calculation is done for the same surface. Agreement between the two is good in general, but the peak at $E = -7.3$ eV(T_1) due to the back-bond surface states occurs at a higher energy compared with the corresponding peak at -8.0 eV in Ref. 15 and is less prominent here. Other minor peaks in Ref. 15 such as D_1, L_1, L_2', R_1, and R_2 are all observable here again. However, as they are relatively insignificant, they are not labeled. $E_F - E_v$ is 0.35 eV.

III. ENERGY BAND STRUCTURE OF BULK DIAMOND

The ionic pseudopotential of carbon is derived subject to the constraint that it reproduce both the atomic energy levels given by Herman and Skillman[16] and the experimental ionic energy levels of C^{3+} (C^{4+} core plus one electron).[17]

We were unable to find a local potential which could satisfy the above conditions with acceptable

TABLE I. Parameters entering Eqs. (7) and (8) to define the ionic pseudopotential (in Ry) of C.

s potential		p potential	
a_1	100	b_1	9
a_2	5.68	b_2	4.41
a_3	3	b_3	11.6
a_4	1.5	b_4	1.3
a_5	0.4	b_5	−0.15

accuracy. As there exist no p core orbitals to cancel the strong Coulomb potential felt by $2p$ electrons, it is quite unlikely that a single local pseudopotential can serve as an acceptable effective potential for both $2s$ and $2p$ electrons. We therefore derived two different potentials for s and p states,

$$V_s(r) = \frac{-e^2 z}{r + a_1 \exp(-a_2 r)} - a_3 \exp[-a_4(r - a_5)^2], \quad (7)$$

$$V_p(r) = \frac{-e^2 z}{r + b_1 \exp(-b_2 r)} - b_3 \exp[-b_4(r - b_5)^2], \quad (8)$$

where $z = 4$. The values of the parameters are found in Table I. Despite the fact that V_p and V_s are pseudopotentials, V_p is as deep as -12 Ry and V_s is about -7.5 Ry. These values are to be contrasted to the typical value of $-4 \sim -5$ Ry for[9] Ge or[7] Si (local pseudopotentials). Calculated eigenvalues of C^{3+} and the C atom using the above potentials are compared with values in the literature in Table II. The maxima of $2s$ and $2p$ wave functions occur at the right places compared with the calculations by Herman and Skillman.[16] The comparison is also given in Table II. $V_{NL} = (V_p - V_s)P_1$ is the required nonlocal part of our pseudopotential, where P_1 is the projection operator for the $l = 1$ angular momentum component. The formulation used above for the nonlocal pseudopotential is described in Ref. 18.

We use approximately 45 plane waves for the expansion of the wave functions and another 45 plane waves are included via Löwdin's scheme.[9] These values correspond to cutoff energies of 10.4 and 17 Ry, respectively. In fact, these cutoff energies are too small to make the energy eigenvalues and the total charge density fully convergent. More plane waves could be used if a detailed bulk calculation is desired. However, limited accuracy suffices here since in proceeding to the surface calculation we are severely restricted by the matrix size because of the large unit cell required in our method. Full conver-

TABLE II. Energy levels of C^{3+} and the C atom calculated from the potential in the text are compared with standard references. Also shown are the calculated positions of the first maxima of $r\psi(r)$ for the 2s and 2p orbitals of carbon in comparison with Herman and Skillman.

C^{3+}	Present results	Moore[a]
2s	−4.743 Ry	−4.742 Ry
2p	−4.154	−4.154
3s	−1.967	−1.981
3p	−1.083	−1.083

C	Present results	Herman[b]
2s	−1.0677	−1.0185 Ry
2p	−0.5090	−0.4021

Positions of max. of $r\psi(r)$ of C	Present results	Herman[a]
2s	1.3 a_{Bohr}	1.17 a_{Bohr}
2p	1.25	1.13

[a]Reference 16.   [b]Reference 17.

gence (within 0.1 eV) is reached at the cutoff energies of 19 and 28.5 Ry. These values are beyond our computational limit for the surface calculation. The differences between the results obtained here and the fully convergent results are found to be up to 0.5 eV in the energy eigenvalues throughout the valence band and less than 20% in the total charge density everywhere in the bulk. As for the charge density, the worst deviation (20%) comes from the relatively unimportant antibonding site which is the direction where we do not have enough plane waves to take care of the rapid charge-density modulation over short distances. At the bonding site the deviation is only 7%. We feel this deviation is tolerable for the
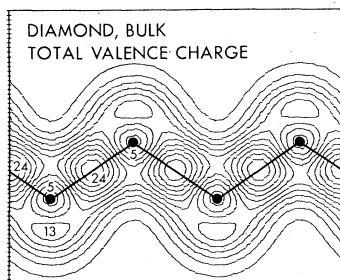

FIG. 8. Total valence charge density of bulk diamond in a (110) plane. The charge density is normalized to the number of electrons per unit-cell volume $\Omega_c = \frac{1}{4} a_c^3$.
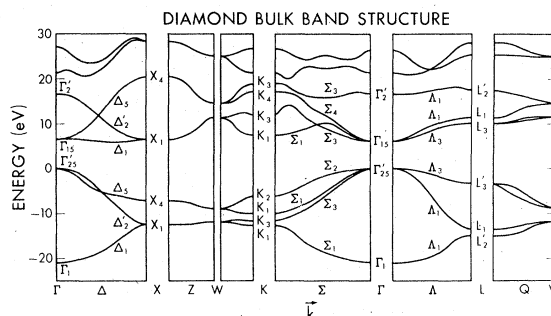

FIG. 9. Band structure of bulk diamond along symmetry lines. The labeling for W is omitted since W has only one two-dimensional irreducible representation W_3.

purpose of the surface calculation in Sec. IV.

The total valence charge density is shown in Fig. 8. This figure just shows a typical charge distribution of a covalent bonding material. Figure 9 shows the band structure for bulk diamond. The indirect gap is 5.7 eV compared with the experimental value of 5.47 eV,[19] and the position of the conduction band minimum occurs at $(2\pi/a_c)$ (0.7, 0, 0) where a_c is the lattice constant, compared with the experimental determination of $(2\pi/a_c)$ (0.78, 0, 0).[20] The valence bandwidth is 20.6 eV, which is consistent with other calculations,[21-27] especially with Painter's results (21 eV).[21] This value is in remarkable agreement with the x-ray K emission[28] or the x-ray photoemission spectroscopy (XPS) measurements (~21 eV).[29] Another XPS experiment[30] reported a somewhat larger bandwidth, 24 eV, but experimental uncertainties are still as great as an eV in these experiments.

IV. DIAMOND (111) SURFACE

The calculational procedure is similar to that described for Ge. The differences are that the potential is nonlocal and the energy cutoffs at 10.4 and 17 Ry now correspond to ~380 plane waves in the basis set and another ~300 plane waves brought in through Löwdin's scheme.[9]

Results are presented in Figs. 10–13 in the same fashion as in Sec. II. We obtained the diamond work function $W \sim 7$ eV with an estimated error of 10%. This value is large compared with the experimental results for graphite (ranging from 4.4 to 4.8 eV).[31-33] There exist no experimental data for the work function of diamond to our knowledge. However, we would expect that the work function of diamond is larger than that of graphite because the valence electrons in diamond are more tightly bound.

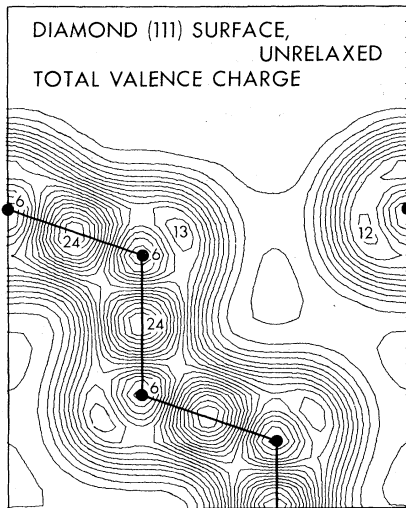Dangling-bond states are shown in Fig. 12. They

FIG. 10. Total charge distribution for an unrelaxed diamond (111) surface in a $(1\bar{1}0)$ plane intersecting the (111) surface at right angles. Normalization is the same as in Fig. 1. Notice that the contour interval is taken to be 1.2 in this figure only.

FIG. 12. Charge density plots for dangling-bond states at Γ, M, and K. Normalization is the same as in Fig. 4.

Back-bond states in the upper valence band are also more strongly localized at the bonding sites; otherwise, they are of the same character as the corresponding states of Ge and are not presented here. One surface state band at low energy is apparently missing here compared with Ge as mentioned in Sec. II. These states merge into the bulk bands because of the strong carbon potential.

are much more localized at the dangling-bond sites than either Ge in Sec. II or Si in Ref. 1. They lie in the lower half of the gap and the bandwidth is ~0.2 eV. Other authors have estimated a much bigger bandwidth (>1 eV).[34,35] Such a small dispersion in our calculation is apparent in Fig. 12, where we can observe strong localizations of charges, hence weak interactions between surface charges. The bandwidth increases when relaxation takes place. Considering the fact that the bandwidth increases from 0.4 to 0.6 eV for the Ge (111) surface, we expect the bandwidth should be within a few tenths of an eV even if relaxation is taken into account.
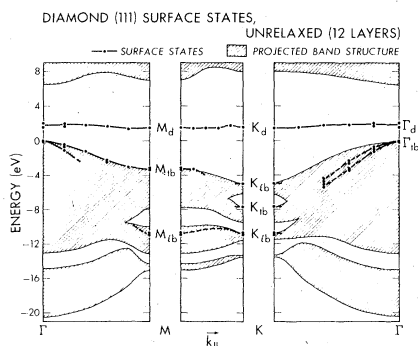

FIG. 11. Two-dimensional band structure of a 12-layer diamond (111) slab along symmetry lines. Surface states and the projected band structure are indicated as in Fig. 2.
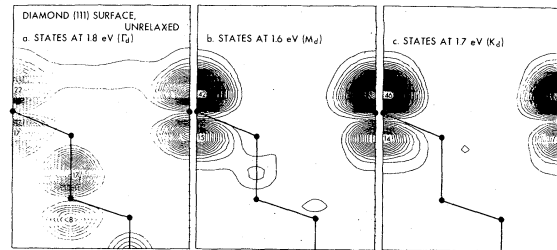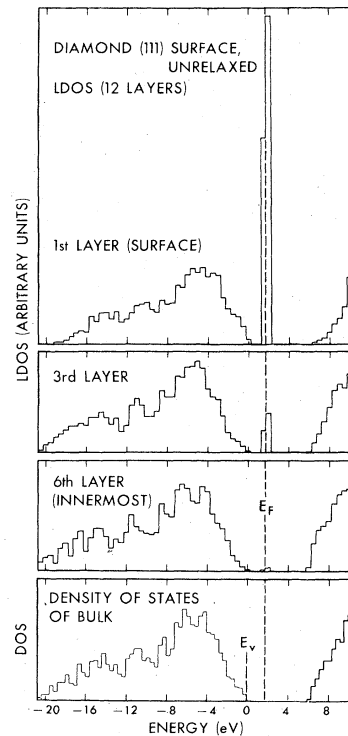

FIG. 13. Local density of states (LDOS) curves for diamond (111) slab. Density of states (DOS) of the bulk calculated in Sec. III is also drawn for comparison. It can be observed that by the third layer, the LDOS is very similar to the bulk DOS except for the gap states. (A portion of charges from both sides of the gap participates in forming surface states in the gap.)

The same is true for Si (unrelaxed) in Ref. 1.

The local density of states is plotted in Fig. 13. The total density of states of bulk diamond obtained from the calculation in Sec. III is also shown. This histogram agrees very well with that of Painter's,[21] but the experimental curves[28-30] show that there is still a nontrivial discrepancy between the experimental and theoretical density of states of diamond and also between experiments.

$E_F - E_v$ is found to be 1.7 eV. E_F falls in the band of the dangling-bond states again, so this ideal surface is metallic. Reconstruction is possible to form a semiconductor surface and we hope these calculations will stimulate experimental studies to decide on the geometry and on the electronic configurations.

Summarizing, the dangling-bond gap states are found and E_F falls in the gap states for Ge, Si,[1] and diamond (111) ideal surfaces. Transverse back-bond states exist at the top of the bulk valence-band edge for both Ge and diamond, whereas the same states lie almost 1 eV below this edge for Si.[1] This does not seem to be explained by the difference in band structures near the gap. However, the difference in energy between the level Γ_d and the level Γ_{tb} does have a definite trend; the differences are 0.7, 1.5, and 1.8 eV for Ge, Si and diamond, respectively. Longitudinal back-bond states around $K(K_{1b})$ are found close to the top of the valence band for Ge, Si, and diamond. Longitudinal back-bond states lying at the center of the valence band are found in a larger region of the BZ (around M and K) and make a finite peak in the LDOS curve for all three materials. Transverse back-bond states in the lower valence band were discussed above.

ACKNOWLEDGMENT

*Research was supported in part by NSF Grant No. DMR76-20647 and under the auspices of the U. S. ERDA.

†Present address: IBM Watson Research Center, P. O. Box 218, Yorktown Heights, N.Y. 10598.

[1]M. Schlüter, J. R. Chelikowsky, S. G. Louie and M. L. Cohen, Phys. Rev. B 12, 4200 (1975).

[2]D. E. Eastman and W. D. Grobman, Phys. Rev. Lett. 28, 1378 (1972).

[3]R. Ludeke and A. Koma, Phys. Rev. B 13, 739 (1976).

[4]P. W. Palmberg and W. T. Peria, Surf. Sci. 6, 57 (1967).

[5]G. Chiarotti, S. Nannarone, R. Pastore, and P. Chiaradia, Phys. Rev. B 4, 3398 (1971).

[6]J. E. Rowe and H. Ibach, Phys. Rev. Lett. 31, 102 (1973); 32, 421 (1974).

[7]M. L. Cohen, M. Schlüter, J. R. Chelikowsky, and S. G. Louie, Phys. Rev. B 12, 5575 (1975).

[8]J. A. Appelbaum and D. R. Hamann (unpublished). See Ref. 9 for details. See also J. A. Appelbaum and D. R. Hamann, in Physics of Semiconductors, edited by M. Pilkuhn (Tuebner, Stuttgart, 1974), p. 681.

[9]J. R. Chelikowsky, Phys. Rev. B 15, 3236 (1977).

[10]M. L. Cohen and V. Heine, Solid State Physics, edited by H. Ehrenreich, F. Seitz, and D. Turnbull (Academic, New York, 1970), Vol. 24, p. 37.

[11]T. Murotani, K. Fujimara, and M. Nishijima, Phys. Rev. B 12, 2424 (1976).

[12]G. W. Gobeli and F. G. Allen, Surf. Sci. 2, 402 (1964).

[13]See, for example, E. Caruthers, L. Kleinman, and G. P. Alldredge, Phys. Rev. B 9, 3330 (1974).

[14]K. C. Pandey and J. C. Phillips, Phys. Rev. Lett. 32, 1433 (1974).

[15]D. J. Chadi and M. L. Cohen, Phys. Rev. B 11, 732 (1975).

[16]F. Herman and S. Skillman, Atomic Structure Calculations (Prentice-Hall, Englewood Cliffs, 1963). Values found in Table II are obtained without tail corrections and with $\alpha = 0.794$. There is agreement with

in 0.04 Ry if correlation is included in Herman and Skillman.

[17]C. E. Moore, Atomic Energy Levels, Natl. Bur. Stand. Circ. No. 467 (U.S. GPO, Washington, D. C., 1949), Vol. 7.

[18]J. R. Chelikowsky and M. L. Cohen, Phys. Rev. B 14, 556 (1976).

[19]C. D. Clark, P. J. Dean, and P. V. Harris, Proc. R. Soc. A 277, 312 (1964).

[20]P. J. Dean and E. C. Lightowlers, Phys. Rev. A 140, 352 (1965); E. O. Kane, ibid. 146, 558 (1966).

[21]G. S. Painter, D. E. Ellis, and A. R. Lubinsky, Phys. Rev. B 10, 3610 (1971).

[22]F. Herman, R. L. Kortum, and C. D. Kuzlin, Int. J. Quantum Chem. 15, 533 (1967).

[23]L. Saravia and D. Brust, Phys. Rev. 170, 683 (1968).

[24]R. Keown, Phys. Rev. 150, 568 (1966).

[25]T. K. Bergstresser and M. L. Cohen, Phys. Rev. Lett. 16, 354 (1966).

[26]R. C. Chaney, C. C. Lin, and E. E. Lafon, Phys. Rev. B 3, 459 (1971).

[27]L. A. Hemstreet, Jr., C. Y. Fong, and M. L. Cohen, Phys. Rev. B 2, 2054 (1970).

[28]M. Umeno and G. Wiech, Phys. Status Solidi B 59, 145 (1972).

[29]T. Gora, R. Staley, J. D. Rimstidt, and J. Sharma, Phys. Rev. B 5, 2309 (1972).

[30]F. R. McFeely, S. P. Kowalczyk, L. Ley, R. G. Cavell, R. A. Pollak, and D. A. Shirley, Phys. Rev. B 9, 5268 (1974).

[31]A. Braun and G. Busch, Helv. Phys. Acta 20, 33 (1947).

[32]S. C. Jain and K. S. Krishnan, Proc. R. Soc. A 213, 143 (1952).

[33]R. F. Willis, B. Feuerbacher, and B. Fitton, Phys. Rev. B 4, 2441 (1971).

[34]S. Ciraci, I. P. Batra, and W. A. Tiller, Phys. Rev. B 12, 5811 (1975).

[35]D. Pugh, Phys. Rev. Lett. 12, 390 (1964).